Femtosecond-tunable measurement of electron thermalization in gold

C.-K. Sun

*Department of Electrical Engineering and Computer Science, Research Laboratory of Electronics,
Massachusetts Institute of Technology, Cambridge, Massachusetts 02139
and Division of Applied Sciences, Harvard University, Cambridge, Massachusetts 02138*

F. Vallée

Laboratoire d'Optique Quantique du CNRS, Ecole Polytechnique, 91128 Palaiseau Cedex, France

L. H. Acioli

Departamento de Física, Universidade de Pernambuco, Recife, Pernambuco 50739, Brazil

E. P. Ippen and J. G. Fujimoto

*Department of Electrical Engineering and Computer Science, Research Laboratory of Electronics,
Massachusetts Institute of Technology, Cambridge, Massachusetts 02139*

(Received 3 May 1994; revised manuscript received 8 August 1994)

Femtosecond electron thermalization in metals was investigated using transient thermomodulation transmissivity and reflectivity. Studies were performed using a tunable multiple-wavelength femtosecond pump-probe technique in optically thin gold films in the low perturbation limit. An IR pump beam is used to heat the electron distribution and changes in electron temperature are measured with a visible probe beam at the d band to Fermi-surface transition. We show that the subpicosecond optical response of gold is dominated by delayed thermalization of the electron gas. This effect is particularly important far off the spectral peak of the reflectivity or transmissivity changes, permitting a direct and sensitive access to the internal thermalization of the electron gas. Using a simple rate-equation model, line-shape analysis of the transient reflectivity and transmissivity indicates a thermalization time of the order of 500 fs. At energies close to the Fermi surface, longer thermalization times $\sim 1-2$ ps are observed. These results are in agreement with a more sophisticated model based on calculations of the electron-thermalization dynamics by numerical solutions of the Boltzmann equation. This model quantitatively describes the measured transient optical response during the full thermalization time of electron gas, of the order of 1.5 ps, and gives new insight into electron thermalization in metals.

I. INTRODUCTION

Ultrafast electron interactions in degenerate electron systems directly influence processes that are important for the understanding of many fundamental and technological properties of solids, such as electronic and thermal transport, laser induced desorption and phase transitions. With the advance of femtosecond laser technology, time-resolved techniques have emerged as powerful tools for the investigation of transient nonequilibrium electron effects in semiconductors and metals. In metals, because of the large difference between the electronic and lattice heat capacities and the possibility of selectively perturbing the electron gas, femtosecond spectroscopy provides the opportunity to separate the electronic and lattice response and to directly monitor the electron-thermalization dynamics.

In femtosecond investigations of metals, a short optical pulse is used to excite the electron distribution out of equilibrium on a time scale much shorter than the electron-phonon interaction time.[1-3] The internal thermalization of the electron gas and equilibration of the electronic and lattice temperature (external thermalization) are subsequently monitored in the time domain using a femtosecond probe pulse. In transient reflectivity and transmissivity studies with ultrashort pulses, the electron-gas relaxation dynamics are analyzed by probing the transient changes of the optical properties of the samples. These techniques were used by several different groups and applied to various metallic systems.[4-14] Because of the large electron population, electron-electron interactions were assumed to be fast enough to thermalize the electron gas on a time scale shorter than the laser pulse duration, permitting a simple modeling of the electron-thermalization dynamics using the classical two-temperature model.[1,15] Although some slight deviations from the expected thermalization behavior were observed,[5,12] these studies did not account for the possibility of creating non-Fermi electron distributions. On the basis of this hypothesis, important information on electron-phonon interaction in metals and metallic superconductors[11,16] and on hot-electron transport in thin me-

     <u>50</u>   15 337

tallic films were obtained.[12]

Recently, direct measurement of the transient electron distribution excited by a femtosecond laser pulse has been performed using photoemission measurements.[17,18] In contrast to the previous assumption, in the high excitation limit (for changes of the electron temperature of the order of 400 K) in gold films, a broad, long-lived photoexcited electron distribution was observed with electron-thermalization time of the order of 600 fs. Taking advantage of the surface plasmon-polariton resonance, evidence for non-Fermi distributions was found at much lower laser fluence by analyzing the temperature dependence of the optically measured electron-phonon interaction time in noble metals.[10] This indirect measurement of the non-thermalized distribution yielded a relaxation time ~ 700 fs in gold, comparable with the electron-phonon relaxation time (~ 1 ps).

Studies of transient thermoreflectivity and thermo-transmissivity measurements in optically thin gold film in the very low perturbative regime have recently shown that the internal thermalization of the electron gas plays a central role in the transient optical properties of metals and strongly modifies their response on a subpicosecond time scale.[19] In contrast to most of the previous experiments, measurement were performed using a multiple-wavelength femtosecond pump-probe technique where an infrared femtosecond pulse perturbed the electron gas and the changes of the optical properties of the metal were probed with a visible pulse at the peak of the reflectivity change (2.48 eV in gold). The use of widely separated pump and probe wavelengths is essential to avoid any influence of the d-band electrons on the measured metal response and permits a more definitive measurement of the electron dynamics. In addition, in the very low perturbative regime, the system response is linear and the measured changes in reflectivity and transmissivity can be related to the electron distribution.

In order to quantitatively investigate the thermalization dynamics of non-Fermi electron distributions and the effects of finite electron-electron scattering time, we have extended these low perturbation measurements using a tunable femtosecond probe. The transient optical properties of a thin gold film have been studied by tuning the probe wavelength in the vicinity of the d band to the Fermi energy transition. We show that far off the spectral peak of the reflectivity or transmissivity changes, the short time (<1 ps) response of the metal is dominated by the nonthermal character of the electron distribution, allowing a direct and very sensitive access to the internal thermalization of the electron gas. To account for the noninstantaneous internal thermalization of the electron gas, we have developed a simple rate-equation model based on a generalization of the two-temperature model.[1,15] This crude energy-exchange-based model which separates the electron-gas fluctuation into thermalized and nonthermalized components has the advantage of giving a qualitative understanding of the observed transient reflectivity and transmissivity changes. A more exact model has also been developed based on numerical solutions of the Boltzmann equation. In association with a band-structure model for gold including the d-band

curvature, this model gives a very good description of the measured data over the full wavelength range investigated.

Experiments were performed using a Ti:Al$_2$O$_3$ femtosecond laser which was frequency doubled to probe reflectivity and transmissivity changes close to the d band to the Fermi-surface transition (~ 2.4 eV in gold). The high stability, high repetition rate and tunability of this laser makes it particularly suitable for our low pump fluence perturbative measurements. A related multiple-wavelength femtosecond technique using an amplified colliding-pulse modelocked (CPM) dye laser has been used to investigate the transient reflectivity of optically thick gold film.[5] However, because of the low repetition rate (8 kHz) and lower stability of the laser system, measurements were performed only for very large perturbations of the electron gas ($\Delta T_e \sim 1000$ K) and with a visible pump pulse (2.0 eV) which could perturb the lower-lying d bands of the probed transition. Theoretical modeling of electron dynamics is thus difficult and the measured temporal behaviors are not directly comparable to these measured in the low perturbation limit with infrared pump pulses.[19]

II. THEORETICAL MODELS

Femtosecond thermomodulation transmissivity and reflectivity in metals rely on measuring transient changes in the optical properties, produced from the perturbation of the electron population by a short pump pulse. On a time scale of the order of the pump pulse duration, a large change in the electron distribution is induced without changes of the lattice temperature. If the energy of the pump photons is much smaller than the energy for the d band to the Fermi-surface transition (2.4 eV in gold), no interband transition is induced. Energy transfer from the laser to the electron gas occurs only through free-carrier absorption, without perturbing the d-band electrons. A broad non-Fermi distribution with energies up to the pump photon energy above the Fermi level is thus created. The density of states of gold is almost constant in the vicinity of the Fermi energy,[20,21] and the electron distribution change $\Delta\rho_{\rm NT}$ for instantaneous excitation and small perturbation can be written

$$\Delta\rho_{\rm NT} = \Delta\rho_{\rm NT}^0 \{ f_0(E - E_p)[1 - f_0(E)]$$
$$- f_0(E)[1 - f_0(E + E_p)] \} , \qquad (1)$$

where E is the electron energy, f_0 is the Fermi distribution at the initial sample temperature T_0 (~ 300 K in our experiments), and E_p is the pump photon energy (with 1.16 eV $< E_p <$ 1.41 eV in our experiments). The amplitude of the population change $\Delta\rho_{\rm NT}^0$ depends on the intensity of the pump. In an optically thin sample (on the order of the skin depth), electronic transport normal to the film occurs within few tens of femtoseconds[12] and will smooth out any longitudinal inhomogeneity in the electron distribution by the end of the pump pulse, leading to a broad spatially homogeneous non-Fermi distribution.

After excitation, energy is redistributed among the electrons through electron-electron interactions, eventu-

ally leading to a hot Fermi distribution with temperature $T_e > T_0$. Figure 1 shows the instantaneous nonthermal population change $\Delta\rho_{NT}$ (solid line) and the corresponding thermalized (or Fermi) population change $\Delta\rho_{Th}$ (dashed lines). The relative amplitude is calculated based on an assumption that all the energy stored in the initial nonthermal distribution is redistributed among the thermalized electrons without any loss to the lattice.

After thermalization, and partly during it, the electron gas loses its energy and externally thermalizes with the lattice through electron-phonon scattering. After a few picoseconds, a local equilibrium will be reached at a slightly higher temperature than the initial condition ($T_c = T_l > T_0, T_l$: lattice temperature). This second step in the electron-thermalization process has been extensively studied and allows quantitative measurements of the electron-phonon interaction parameters.[11,16] As a final step in the electron-thermalization, thermal diffusion into the substrate and in the transverse direction will occur, and the electron population will return to the original temperature T_0. This last process occurs on a 100-ps time scale[22] and is not investigated here. The changes of the electron distribution during internal and external thermalization of the electron gas result in modifications of the interband absorption spectrum and consequently the optical properties of the metal film. These changes are maximum close to the energy transition from the top of the d band to the Fermi surface, where larger changes in the occupation numbers are expected.[23,24] Because of the curvature of the d band, the changes in the imaginary part of the dielectric function at a given probe photon energy cannot be directly related to a unique electron energy in the conduction band, but are associated with a range of electron energies whose contributions are weighted by the transition probability. Before modeling the electron-thermalization dynamics, we will briefly summarize the model developed by Rosei *et al.*[23,24] which relates the observed changes of the film reflectivity
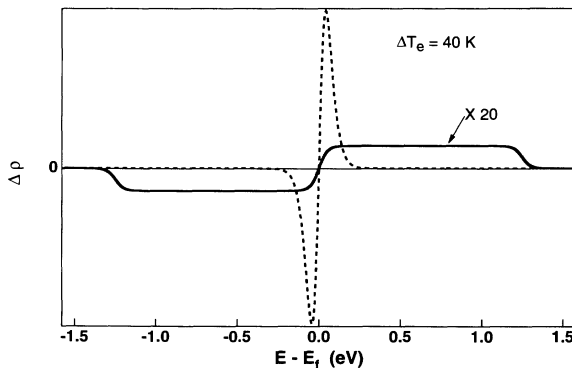
and transmissivity to the changes of the electron occupation number.

A. Transient reflectivity and transmissivity

In order to measure the electron-thermalization dynamics, the changes of the electron distribution have to be related to the changes in the optical properties. In the perturbative regime, the transient differential reflection $\Delta R/R$ and differential transmission $\Delta T/T$ of the sample can be expressed as linear combinations of the induced changes in the real and imaginary part of the dielectric constant $\Delta\epsilon_1$ and $\Delta\epsilon_2$,

$$\frac{\Delta R}{R} = \frac{\partial \ln R}{\partial \epsilon_1}\Delta\epsilon_1 + \frac{\partial \ln R}{\partial \epsilon_2}\Delta\epsilon_2 , \tag{2a}$$

$$\frac{\Delta T}{T} = \frac{\partial \ln T}{\partial \epsilon_1}\Delta\epsilon_1 + \frac{\partial \ln T}{\partial \epsilon_2}\Delta\epsilon_2 . \tag{2b}$$

The coefficients of proportionality in these linear expansions can be calculated using the theoretical reflection and transmission formula for thin films.[25] They are functions of the sample thickness and the complex refractive index of the sample at the probe wavelength, which is estimated using an interpolation of the available optical data in gold.[26]

The changes of the real and imaginary parts of the dielectric function can be related to the changes of the electron distribution function by use of the model developed by Rosei and co-workers for cw thermodulation measurements.[23,24] For our probe wavelengths in gold, the main contribution comes from the modification of the absorption associated with the transition from the fully occupied d band to the conduction band in the vicinity of the L point of the Brillouin zone (Fig. 2). Using the constant matrix element approximation, the change of the imaginary part of the dielectric function is given by

$$\Delta\epsilon_2(\hbar\omega) = \frac{1}{(\hbar\omega)^2} \int D(E,\hbar\omega)\Delta\rho(E)dE , \tag{3}$$

FIG. 1. Instantaneous electron distribution change $\Delta\rho_{NT}$ (solid line) created by free-carrier absorption of an infrared pump pulse and corresponding thermalized electron distribution change $\Delta\rho_{Th}$ (dashed line), 20 times amplified vs electron energy E. The infrared photon energy E_p and the initial sample temperature T_0 were assumed to be 1.25 eV and 300 K, respectively. The same energy is stored in the two distributions corresponding to a 40-K electron temperature rise.
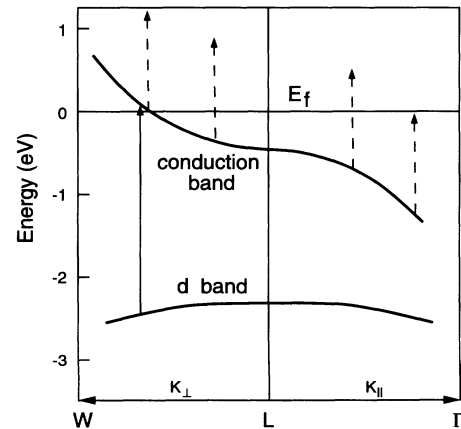
FIG. 2. Simplified parabolic band-structure model of gold in the vicinity of the L point of the Brillouin zone (from Ref. 23). Arrows with solid lines represent the probe transitions. Arrows with dashed lines represent the pump transitions.

where $D(E,\hbar\omega)$ is the joint density of states with respect to the energy E of the final state in the conduction band

$$D(E,\hbar\omega)=\frac{1}{(2\pi)^3}\int 'd^3k\,\delta[E_c(\mathbf{k})-E_d(\mathbf{k})-\hbar\omega]$$

$$\times\delta[E-E_c(\mathbf{k})]\ .\qquad(4)$$

$D(E,\hbar\omega)$ is calculated assuming parabolic band structures for the d bands and conduction band in the vicinity of the L point of the Brillouin zone with the parameters given in Ref. 23. This fully determines $\Delta\epsilon_2$ as a function of the differential electron occupation number. The change of the real part of the dielectric constant $\Delta\epsilon_1$ is computed using the Kramers-Kronig relationship.

Using (2) and (3), the reflectivity and transmission changes can thus be readily connected to the electron distribution function. This is exemplified in Fig. 3 showing the computed probe wavelength dependence of $\Delta R/R$ and $\Delta T/T$ for a 200 Å gold sample between 2.1–2.8 eV. The solid and dashed lines are calculated, respectively, for the non-Fermi and Fermi perturbation ($\Delta T_e=40$ K) of Fig. 1, with the same excess energy stored in the two distributions. For a thermal distribution, the width of the calculated shape is dominated by the curvature of the d bands and is almost insensitive to the electron temperature change up to $\Delta T_e=100$ K. The spectral shape for the nonthermal distribution change is much flatter and wider because of the broad electron occupancy changes in the non-Fermi distribution. Conversely, the peak amplitude for the thermal perturbation is much larger than for the nonthermal perturbation.

Because of the striking differences in the line shapes of the spectral responses, we expect to observe complex temporal behavior depending on the probe wavelength. At probe photon energies close to the peak of the thermalized response, the contribution from the thermalized electrons is expected to dominate. Tuning the probe wavelength either through the zero of the thermalized response or far off the peak of the response, the contribution from the thermalized electrons should be reduced, leading to the direct observation of the internal thermali-

zation of the electron gas. For a thicker sample, the spectral dependence of the differential transmissivity and reflectivity is similar to those in a 200-Å film with a shift toward shorter wavelength due to the thickness dependence of the coefficients in (2).

B. Rate-equation model

Because of the very small electron density initially perturbed by the pump pulse, a phenomenological description of the electron gas can be obtained by separating the electron distribution into a high-density thermalized distribution and a very-low-density nonthermalized distribution.[18,19] Neglecting particle exchange, this last component decays by energy exchange with the Fermi component, acting as a heat reservoir. If only energy redistribution is considered, the electron gas can be described through its energy content and the evolution of the electron-phonon coupled system can be modeled by extending the two-temperature model using three coupled differential equations,

$$\frac{\partial N}{\partial t}=-\alpha N-\beta N\ ,\qquad(5a)$$

$$\frac{C_e\partial T_e}{\partial t}=-G(T_e-T_l)+\alpha N\ ,\qquad(5b)$$

$$\frac{C_l\partial T_l}{\partial t}=G(T_e-T_l)+\beta N\ ,\qquad(5c)$$

where C_e and C_l are the electronic and lattice heat capacities, T_l is the lattice temperature, G is the electron-phonon coupling constant, N stands for the energy density stored in the nonthermalized part of the distribution, α is the electron gas heating rate, and $\beta=G/C_e$ is the electron-phonon coupling rate. The last term in (5b) αN describes heating of the electron gas by the initial nonthermalized electrons and βN represents the direct coupling between these nonthermalized electrons and the lattice. Combining (5b) and (5c), we get

$$\frac{\partial(T_e-T_l)}{\partial t}=-\beta'(T_e-T_l)+\left[\frac{\alpha}{C_e}+\frac{\beta}{C_l}\right]N\qquad(6)$$

with $\beta'=G(1/C_e+1/C_l)$. For our experimental conditions $C_l\gg C_e$ which means that β' and β can be identified and the difference between the initial and equilibrated lattice temperature is small, $T_l\sim T_0$.

For perturbative temperature changes ($\Delta T_e\ll T_0$), C_e and G can be considered as constants, leading to the description of the electron-phonon evolution by a simple set of linear equations. The transient energy in the electron system ($N,\Delta T_e C_e$) can thus be described by response functions with the form

$$N\propto H(t)\exp\left[\frac{-t}{\tau_{\text{th}'}}\right]\ ,\qquad(7a)$$
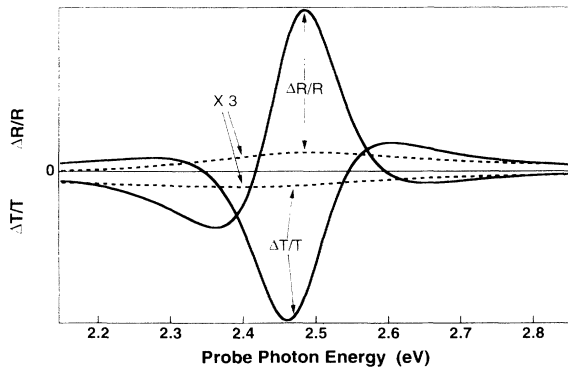

FIG. 3. Calculated probe photon energy dependence of $\Delta T/T$ and $\Delta R/R$ for a 200-Å-thick gold film for the initial nonthermalized electron distribution (dashed lines, three times amplified) $\Delta\rho_{\text{NT}}$ and thermalized electron distribution (solid lines) $\Delta\rho_{\text{Th}}$ of Fig. 1.

$$\Delta T_e C_e \propto \Delta T_e \propto H(t) \left[1 - \exp\left[\frac{-t}{\tau_{\text{th}}} \right] \right] \exp\left[\frac{-t}{\tau_p} \right] \quad (7b)$$

with $\tau_p = 1/\beta$, $\tau_{\text{th}} = 1/\alpha$, and $\tau_{\text{th}'} = 1/(\alpha+\beta)$. $H(t)$ is the Heaviside function and we define τ_{th} as the thermalization time. Equations (7a) and (7b) show a delayed rise of the temperature of the thermalized electron population with time constant τ_{th}, and an accompanied decay of the energy stored in the nonthermal distribution. The temperature of the thermalized distribution decays due to electron-phonon interaction with a time constant τ_p. The rise time of the thermalized distribution τ_{th} being longer than the decay time of nonthermal population $\tau_{\text{th}'}$ reflects the fact that the non-thermalized electron distribution interacts with the phonon bath during the thermalization process.

For the very small induced temperature changes in our experiments, the contribution of the thermalized distribution to the transient reflection and transmission is directly proportional to the electron temperature change (7b). This component dominates for probe wavelengths close to the peak reflectivity or transmissivity changes (Fig. 3) and (7b) gives a good description of both the transient reflectivity and transmissivity.[19] Far off this probing range, the nonthermal distribution contributes significantly to the optical changes which depend on both the integrated energy and the shape of the electronic distribution, rendering the description of electron dynamics more complicated. As a crude approximation, we generalized the previous approach and introduce the contribution of the nonthermal electrons by a term proportional to their integrated energy density N. This approach which describes the nonthermal electron distribution by a unique energy-associated time constant, is equivalent to using a time-averaged electron distribution function and reduces the influence of the high-energy electrons. With this approximation, the response function at the probe photon energy $\hbar\omega$ can be expressed as

$$\frac{\Delta R}{R}(\hbar\omega, t) = H(t) \left\{ \frac{\Delta R}{R}\bigg|_{\text{NT}} (\hbar\omega) \exp\left[\frac{-t}{\tau_{\text{th}'}} \right] \right.$$

$$+ \frac{\Delta R}{R}\bigg|_{\text{Th}} (\hbar\omega) \left[1 - \exp\left[\frac{-t}{\tau_{\text{th}}} \right] \right]$$

$$\times \exp\left[\frac{-t}{\tau_p} \right] + \frac{\Delta R}{R}\bigg|_L (\hbar\omega) \bigg\} \quad (8)$$

with a similar expression for $\Delta T/T$. The term $\Delta R/R|_L(\hbar\omega)$ is added to account for the small residual electronic and lattice contributions due to the difference between the initial sample temperature and the equilibrated electron-phonon temperature before diffusion.[19]

Although this approach neglects the energy dependence of the electron relaxation, it permits a simple, qualitative description of the electron dynamics. With the exception of some small discrepancies, this model yields remarkable agreement with the experimental results.

C. Numerical model

The rate-equation model described above gives a simplified global description of the electron distribution dynamics through the redistribution of the injected energy. A more exact model must take into account the local kinetics of the electron occupation number. This can be calculated by solving the Boltzmann equation for the electrons

$$\frac{df(\mathbf{k})}{dt} = \frac{df(\mathbf{k})}{dt}\bigg|_{e\text{-}e} + \frac{df(\mathbf{k})}{dt}\bigg|_{e\text{-ph}} + I(\mathbf{k}, t), \quad (9)$$

where $f(\mathbf{k})$ is the occupation number of the $\mathbf{k}$ electronic state and $I(\mathbf{k}, t)$ stands for the perturbation of the electron gas by the pump pulse. The electron scattering rate due to electron-electron collision takes the usual form

$$\frac{df(\mathbf{k})}{dt}\bigg|_{e\text{-}e} = \frac{2\pi}{\hbar} \sum_{k_1, k_2, k_3} \{ M^2(\mathbf{q}) f(\mathbf{k}_2) f(\mathbf{k}_3) [1 - f(\mathbf{k}_1)(1 - f(\mathbf{k})] \delta(\mathbf{k}_2 + \mathbf{k}_3 - \mathbf{k}_1 - \mathbf{k}) \delta(E_2 + E_3 - E_1 - E)$$

$$- M^2(\mathbf{q}) f(\mathbf{k}) f(\mathbf{k}_1) [1 - f(\mathbf{k}_2)] [1 - f(\mathbf{k}_3)] \delta(\mathbf{k} + \mathbf{k}_1 - \mathbf{k}_2 - \mathbf{k}_3) \delta(E + E_1 - E_2 - E_3) \}, \quad (10)$$

where the first and second term correspond, respectively, to scattering in and out of the $\mathbf{k}$ state. Here $M(\mathbf{q})$ is the scattering amplitude with momentum exchange $\mathbf{q} = \mathbf{k} - \mathbf{k}_2 = \mathbf{k}_3 - \mathbf{k}_1$. In noble metals, the conduction electrons can be adequately treated as free electrons and we will use this approximation in the following. Using a standard procedure, integration over the direction of the wave vectors can be analytically performed and the electron-electron scattering rate can be transformed into an energy dependent expression.[27] The equation is then solved numerically using 1-meV steps and describing electron-electron interaction by a static screened Coulomb interaction potential

$$M(q) = \frac{e^2}{V\epsilon} \frac{1}{q^2 + k_0^2}, \quad (11)$$

where k_0 is the inverse screening length. For a very-high-density electron gas, k_0 can be calculated using the static Lindhard model for screening.[28] However, in order to simplify the numerical solutions of the Boltzmann equation, we assume an average screening length which is treated as an adjustable parameter. Because of the small temperature changes in our measurements and due to the fast decay of high-energy electron by electron-electron collisions, the electron-phonon collision rate is introduced in the relaxation time approximation

$$\left. \frac{df(\mathbf{k})}{dt} \right|_{e-\text{ph}} = \frac{[f_0(\mathbf{k}) - f(\mathbf{k})]}{\tau_p} , \qquad (12)$$

where the small change between the initial and final lattice temperature has been neglected. τ_p was defined in (7b). The electron-phonon coupling parameter has been previously measured and in the weak perturbation regime we will use $\tau_p = 1$ ps.[19] Combining the electron distribution kinetics calculated numerically and the model of Sec. II A, the transient differential reflectivity and transmissivity can be calculated as a function of probe wavelength. This is exemplified in Fig. 4 where the temporal evolution of $\Delta R / R$ in a 200-Å gold film has been plotted for different probe energies in the vicinity of the peak change, assuming an instantaneous thermalization of the electron gas ($\Delta T_e = 40$ K). As will be shown later, this hypothesis of instantaneous thermalization does not adequately describe our experimental results.

III. EXPERIMENTAL SETUP

Femtosecond pump and probe measurements of transient reflection and transmission were performed using a tunable multiple-wavelength technique. The experimental configuration is shown schematically in Fig. 5. The laser source used for these studies was a Kerr Lens Modelocked Ti:Al$_2$O$_3$ laser (Coherent Mira 900) which generated 120–150-fs pulses in the wavelength range 1.065 μm–880 nm with average energy 200 mW (at 1.065 μm) to 1.6 W (at 905 nm). Measurements were performed using a standard pump-probe geometry. One portion of the infrared beam, with about one-half of the available power, passed through a variable delay stage and was used as the pump beam. The other half of the infrared beam was focused into a 100-μm-thick beta barium borate (BBO) crystal to produce frequency doubled probe pulses tunable within 532.5–440 nm (2.33–2.82 eV), corresponding to the d band to Fermi-surface transition in gold ($\sim$2.4 eV). After the second harmonic crystal, the infrared pulses were removed using a colored glass filter. At 1-μm wavelengths, the average power of the doubled visible beam was 70 μW, and its duration was 210 fs measured at the position of the sample by
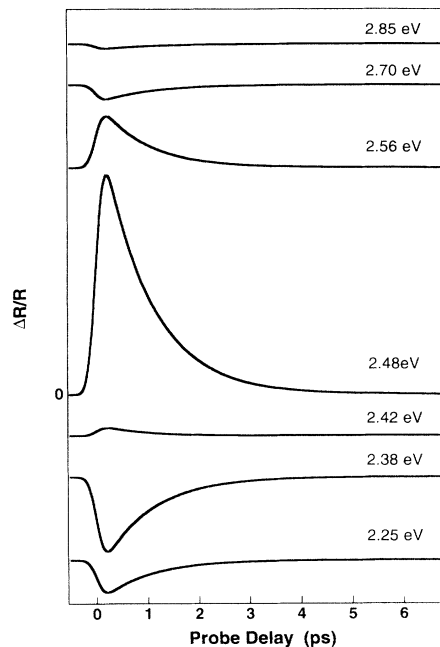

FIG. 4. Calculated temporal dependence of the transient differential reflectivity $\Delta R / R$ in a 200-Å-thick gold film for various probe photon energies, assuming instantaneous internal thermalization of the electron gas with $\Delta T_e = 40$ K.

cross correlation with the pump beam in a second BBO crystal. Since only a very weak probe was necessary, no attempt was made to improve the conversion efficiency which was of the order of 5×10^{-4}.

The pump and probe beam were focused into the sample using a 10$\times$ microscope objective. The focal spot diameter of the IR and visible beams were measured to be 11 and 8 μm, respectively. The pump power was attenuated before the sample to the mW range, corresponding to a fluence of 2.5–100 μJ/cm^2 on the sample to insure that measurements were performed in the perturbative regime. The reflected and transmitted infrared were rejected with irises and colored glass filters so that only the visible probe signals were detected. The pump beam was chopped and a portion of the probe beam before the
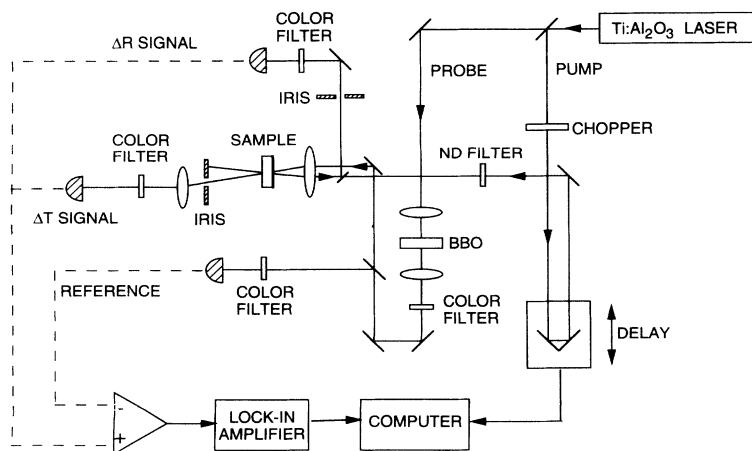

FIG. 5. Multiple-wavelength pump-probe setup.

sample was used as a reference beam. The differential signal between detected probe and the reference was measured as a function of the temporal delay between the pump and probe using a lock-in amplifier.

Within the tuning range of the $Ti:Al_2O_3$, free-carrier absorption can be assumed to be frequency independent and the difference in the initial electron distributions generated by different pump photon energies is negligible. Therefore, the experimental results can be interpreted as probing the evolution of the same initial population by wavelength tunable pulses. The experiments (reflectivity R and transmissivity T) were performed at room temperature (~ 300 K) in a 200-Å-thick polycrystalline gold sample deposited on a sapphire substrate. The thickness of the sample is comparable to the gold skin depth (~ 125 Å at 1 μm^{28}) so that ballistic diffusion of hot electrons can be neglected. In order to investigate the effects of diffusion and sample thickness, experiments were also performed with 400-Å (R, T) and 1200-Å (R only) samples.

IV. RESULTS AND ANALYSIS

The measured $\Delta R / R$ and $\Delta T / T$ in a 200-Å gold film for probe photon energy in the 2.34–2.82-eV range are shown in Figs. 6 and 7 (left figure, solid lines) for a normalized pump fluence of 30 $\mu J/cm^2$. The absorption of the sample has been measured to be $\sim 5\%$, in agreement

FIG. 7. Measured transient transmissivity for different probe photon energies and 30 $\mu J/cm^2$ pump fluence. The arrangement is the same as in Fig. 6.
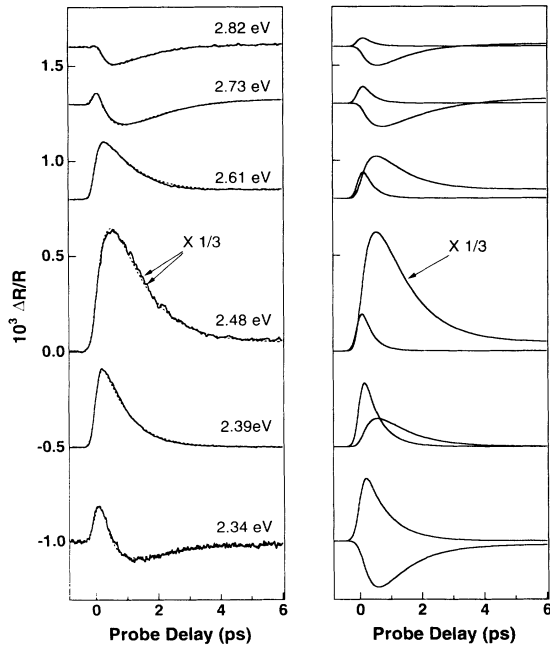

FIG. 6. (Left) Measured transient reflectivity (solid lines) vs probe time delay for probe photon energies ranging from 2.34 to 2.82 eV. The incident pump fluence is 3 $\mu J/cm^2$. The results for different probe energy are vertically displaced for clarity. Dashed lines on top of the results are the generated convolution fits using the rate-equation model of Sec. II B. (Right) Fitted contributions for the nonthermal and thermal parts of the electron distribution corresponding to the first in the left part of the figure.
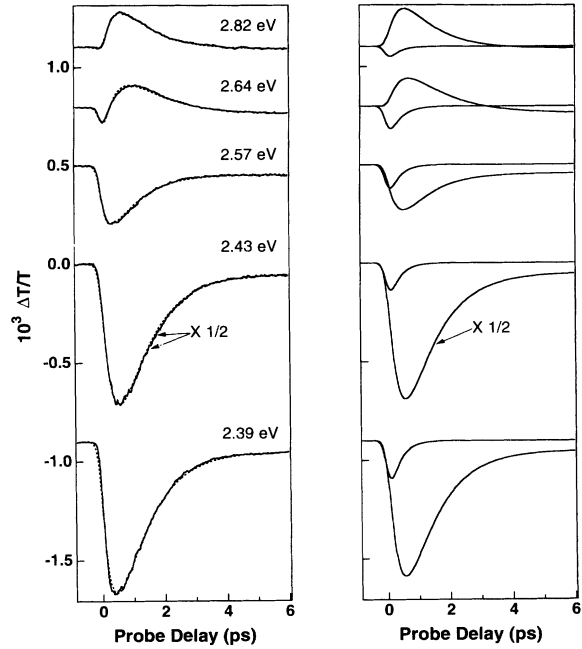
with theoretical predictions based on the known bulk optical constants[26] and the calculated reflection and transmission of a thin film.[25] Assuming that all the absorbed energy is initially stored into the thermalized electron gas, the maximum peak change of the electron temperature ΔT_e^M would be ~ 30 K. Measurements performed at low powers (fluence between 2.5 and 200 $\mu J/cm^2$, i.e., $\Delta T_e^M \sim 3$–200 K) show the same behavior for the measured shape up to a constant scale factor, indicating that the measurements were in the perturbative limit.

The maximum amplitude changes in $\Delta R / R$ and $\Delta T / T$ occur at 2.48 and 2.43 eV, respectively. This shift of the maximum position and the negative sign of $\Delta T / T$ are in agreement with the model of Sec. II (see Fig. 3). Close to these maxima, the transient behavior is characterized by a rise time much longer than the response function of our experimental system, followed by an exponential decay. Comparing the results of the $\Delta R / R$ and $\Delta T / T$, the same response is observed except for the small residual signal at long delay time, indicating that the dynamics of $\Delta \epsilon_1$ and $\Delta \epsilon_2$ are similar. The delay in reaching the maximum signal has been shown to be associated with a delayed thermalization of the electron gas.[19] Using the rate-equation model of Sec. II B and neglecting the contribution of the nonthermal distribution, the same time constants are obtained for the transmissivity and reflectivity data with $\tau_{th} = 500$ fs and $\tau_p = 1$ ps.[19]

For probe photon energies away from the maximum response, the shapes of both $\Delta R / R$ and $\Delta T / T$ become more complex with much faster rise time. In particular, close to the photon energies where the differential reflectivity changes sign (~ 2.7 and ~ 2.35 eV) the signal

displays a fast positive transient, limited by the response function of our system, followed by a negative signal and a slow return to equilibrium. Similar behaviors are observed for the transmissivity measurements. There behaviors are directly related to the noninstantaneous thermalization of the electron gas and can be qualitatively understood by noting that the initial broad photoexcited electron distribution leads to a positive change of the reflectivity over almost the entire probing range while the thermalized distribution corresponds to either a positive or negative signal (Fig. 3). The same behavior is observed around 2.65 eV for the transmissivity measurements, with the opposite sign (Fig. 3) as expected from the calculations outlined in Sec. II, and a shift toward lower probe photon energy. Because of this shift, the low-energy sign change of $\Delta T/T$ has not been observed and is out of the tuning range of our laser.

In order to qualitatively describe the measurements, we have used the simple rate-equation model of Sec. II B. The dashed lines on the left side of Figs. 6 and 7 on top of the experimental measurements are the fitted data for all wavelengths taking both nonthermal and thermal response into account [Eq. (8)]. The time constants are those derived from fitting the peak response, $\tau_{th} = 500$ fs, $\tau_p = 1$ ps, and $\tau_{th'} = 1/3$ ps $(1/\tau_{th'} = 1/\tau_p + 1/\tau_{th})$. These time constants hold for both reflectivity and transmissivity changes over the investigated energy range except for probe photon energies in the 2.34–2.39-eV range. In this range, the probe monitors mainly electron states close to the Fermi energy and a longer "local" thermalization time τ_{th} is required (1–2 ps). This is commensurate with inhibition of electron-electron scattering close to the Fermi surface because of k-space filling, as predicted by the Fermi-liquid theory. The traces on the right-hand side show separately the fitted contributions of the nonthermal and thermal components of the response corresponding to the dashed lines on the left-hand side (including a residual long-lived signal from lattice temperature change). The amplitudes of the response function $\Delta R/R|_{Th}$, $\Delta R/R|_{NT}$, $\Delta T/T|_{Th}$, and $\Delta T/T|_{NT}$ used for the fitting are shown in Fig. 8. Their shapes compare favorably with those calculated in Fig. 3 with a larger amplitude for the nonthermal contribution. This is due to the energy transfer from the nonthermal distribution to the lattice system during the internal thermalization process, the fast decay of the high-energy nonthermal electrons, and the consequent larger occupation number change for electrons close to the Fermi surface than calculated in Fig. 3. The experimental line shape is also found to be narrower than that calculated for the initial instantaneous perturbation of the electron gas (Fig. 3).

Using the numerical model of Sec. II C, we have calculated the transient reflectivity of optically thin gold films. The measured and calculated temporal evolution of $\Delta R/R$ at its peak value (2.48 eV) are plotted in Fig. 9. Apart from the absolute amplitude of the calculated reflectivity change, the inverse screening length k_0 is the only parameter used in the calculations. Here we have used $k_0 = 0.8\ k_{DH}$ where k_{DH} is the Debye-Huckel wave vector. This reduction of the screening compared to the Debye-Huckel model is concomitant with averaging of
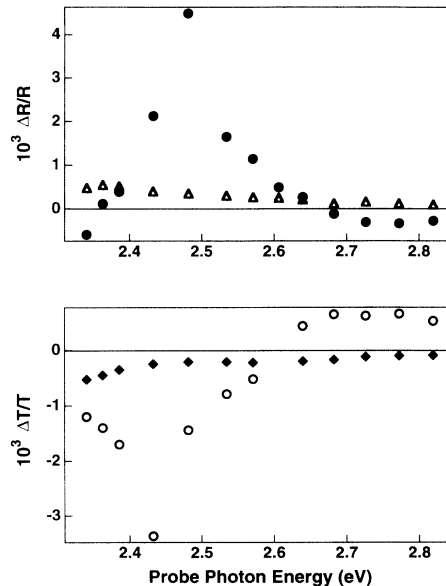

FIG. 8. Probe photon energy dependence of the amplitude of the nonthermal and thermal contribution using the rate-equation model of Sec. II B. (Top) $\Delta R/R|_{Th}$ (closed circles) and $\Delta R/R|_{NT}$ (open triangles). (Bottom) $\Delta T/T|_{Th}$ (open circles) and $\Delta T/T|_{NT}$ (closed diamonds).

the more exact value from the Lindhard theory.[28] Results of the calculations performed at different probe photon energies are displayed in Fig. 10 and show a good agreement with the experimental results, especially close to the change in sign of the reflectivity. Similar agreements are obtained for the transmission changes with a good prediction of the probe wavelength dependence of both the temporal shape and relative amplitude. As suggested by the simple rate-equation model, the slow rise time at 2.48 eV and the fast positive transient around 2.7 and 2.35 eV are direct signatures of the noninstantaneous internal thermalization of the electron gas. This is clear-
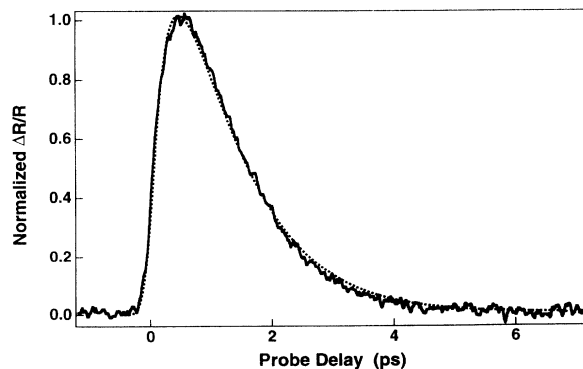

FIG. 9. Measured and calculated transient reflectivity at the peak change. $\Delta R/R$ is calculated at 2.48 eV using the numerical model of Sec. II C. The pump fluence is 14 $\mu J/cm^2$ corresponding to a maximum electronic temperature change ΔT_e^M of 15 K. The weak residual signal due to the small difference between the equilibrated and initial temperatures has been subtracted.
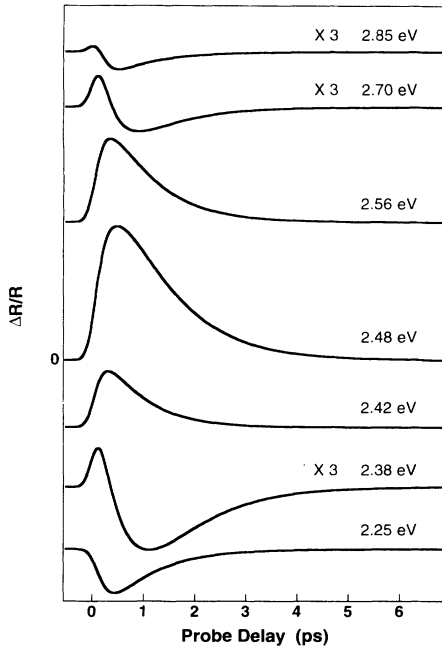
FEMTOSECOND-TUNABLE MEASUREMENT OF ELECTRON . . .

FIG. 10. Calculated temporal dependence of $\Delta R/R$ for various probe photon energies. ΔT_e^M is 40 K and pump fluence is $\sim 30\,\mu J/cm^2$.

ly shown in Fig. 11 which displays the calculated transient reflectivity at 2.68 eV for finite electron-electron interactions and for an instantaneous thermalization of the electron gas, assuming the same injected energy. For an instantaneous thermalized electron distribution, no positive transient peak is calculated and the signal simply decays exponentially by electron-phonon interactions. These two responses become similar for probe time delays longer than 1.5–2 ps for which the electron gas is fully thermalized.

The calculated electron occupation number is shown in Fig. 12(a) for different temporal delays after the perturbation by a 1.25-eV pump with a pulse duration of 140 fs. The high-energy part of the distribution decays very quickly (typically on a 10-fs time scale) raising the occu-
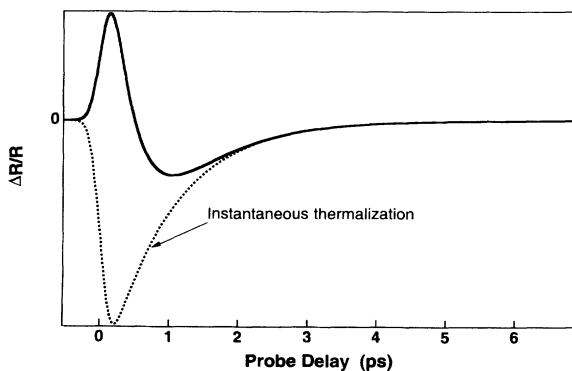

FIG. 11. Calculated $\Delta R/R$ at 2.68 eV using numerical solutions of the Boltzmann equation (solid line) and assuming instantaneous thermalization of the electron gas (dashed line) with $\Delta T_e = 40$ K.

pation number in the vicinity of the Fermi level. This corresponds to a rise of the electron temperature defined in the vicinity of E_F and an increase of number of low-energy electrons which slowly thermalize with the rest of the distribution. This behavior and the slow electron thermalization close to the Fermi energy are in agreement with the Fermi-liquid theory which predicts a quadratic dependence of the relaxation rate with $E - E_F$ (for $E - E_F > kT$). The electron gas is almost fully thermalized after a time delay of 1.5–2 ps to a temperature of 313 K [Fig. 11(a) inset], lower than the peak temperature of 340 K assuming instantaneous thermalization because of energy transfer to the lattice during the internal thermalization process. This thermalization time (1.5–2 ps) is comparable to the temporal delay in reaching the minimum $\Delta R/R$ for probe photon energies around 2.7 and 2.35 eV (Figs. 6 and 10), with a slightly longer time at 2.35 eV for which the signal is more sensitive to the electron distribution in the close vicinity of the Fermi energy.

The calculated spectral shapes of the differential reflectivity are shown in Fig. 12(b) for different time delays. The complex evolution of the response is clearly
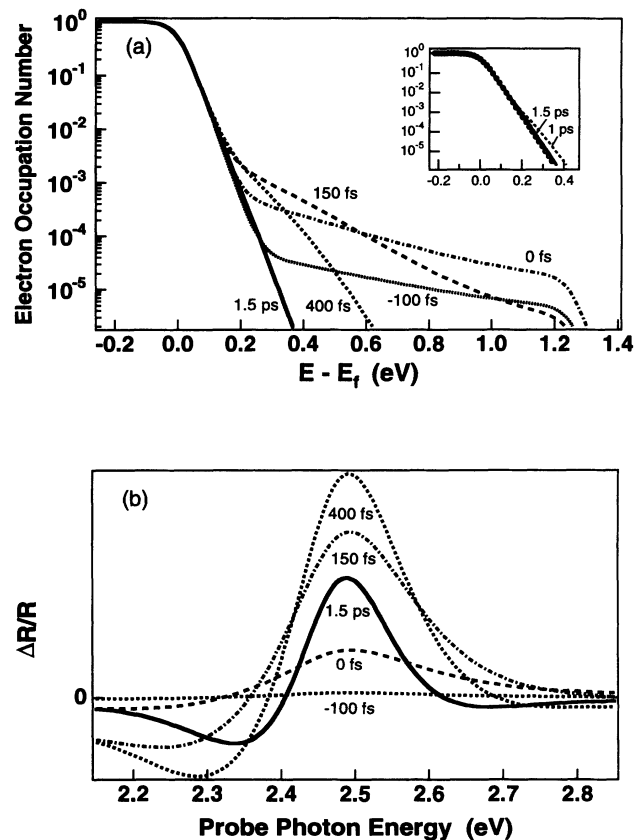

FIG. 12. (a) Calculated electron occupation number for excitation with 1.25-eV photon energy and 140-fs pulse durations for various time delays ($\Delta T_e^M = 40$ K). The inset shows the electron distribution for 1-ps (dashed line) and 1.5-ps delays (solid line) together with a Fermi-Dirac distribution at 313 K (dots). (b) Calculated probe photon energy dependence of $\Delta R/R$ for the electron distribution of Fig. 11(a).

seen in the 2.6–2.8 and 2.3–2.4-eV ranges. Further away from the peak change, the noninstantaneous thermalization of the electron gas contributes strongly to the observed transient signal. In particular in the 2-eV region, the short time delay signal is dominated by the nonthermalized part of the distribution, leading to an almost instantaneous rise time of the reflectivity change, very different from the one measured at the peak $\Delta R/R$ (Fig. 13). Using the rate-equation model interpretation, the thermal and nonthermal contributions are of the same sign and comparable amplitude. These results in fast rising signals which decay exponentially with τ_p after a few hundred fs and no sign changes during the electron-gas thermalization for either reflectivity or transmissivity measurements. This is in agreement with the fast reflectivity rise time observed in previous experiments using a 2-eV probe.[8,9,11,12]

As soon as the electronic temperature is established, the measured signal (proportional to the temperature change in our experimental conditions) is found to decay exponentially independent of the probing energy with a time constant of 1 ps. This is in agreement with previous determination based on an extraction procedure[8] or multiple temperature measurements taking the nonlinearity of effective electron temperature into consideration.[9]

Our estimated overall electron-thermalization time $\tau_{th} = 500$ fs is comparable to the previous estimations.[6,17,18] On the basis of the very high electron density of metals, one would expect a very rapid electron-electron interaction. However, the interaction efficiency is considerably reduced by screening which greatly attenuates the efficiency of the Coulombic interaction and by phase space filling which blocks most of the energetically possible interaction channels. This last mechanism seems to be dominant in delaying the thermalization of electrons close to the Fermi energy (Fig. 12) in agreement with Fermi-liquid theory. For electrons 1 eV above the Fermi level, which is close to the maximum energy of the pump induced non-Fermi electrons, an electron-electron scattering time on the order of 100 fs can be estimated from mean-free-path measurements.[29] Closer to the Fer-

mi energy, this time is even longer and an overall thermalization time of a few hundred fs can be estimated.[6,17] Inhibition of the electron-electron interactions is a common feature of degenerated systems and has also been observed in bulk semiconductors[30] and modulation doped quantum-well semiconductors, where carrier dephasing times in the picosecond range were measured.[31]

The effect of pump fluence for reflectivity measurement at 925 nm (probe photon energy 2.68 eV) is shown in Fig. 14(a). The two different curves, which correspond, respectively, to 50 and 500 $\mu J/cm^2$ pump fluence, show different temporal behavior. For higher temperature changes, induced by stronger pump fluence, the thermalized distribution contributed $\Delta R/R$ line shape broadens while the contribution from the nonthermal electrons remains identical. This difference results in different ratio between the thermal and nonthermal response at this probe frequency and different transient responses at two different pump fluence, reflecting the temperature dependent line shapes for the thermalized Fermi population. The calculated changes are in good qualitative agreements with the observed data, reproducing in particular the modification of the temporal shape with pump fluence [Fig. 14(b)].

The transient optical properties were also measured for the same probe photon energy range, 2.34–2.82 eV, in 400- and 1200-Å samples. In the 400-Å sample, almost the same behavior was observed as in the 200-Å sample with similar spectral line shapes and smaller amplitudes due to longitudinal electron transport. The spectral shapes are shifted toward higher photon energy, in agreement with the predictions of the model calculations. This shift is due to the thickness dependence of the reflection and transmission of thin films, which results in different
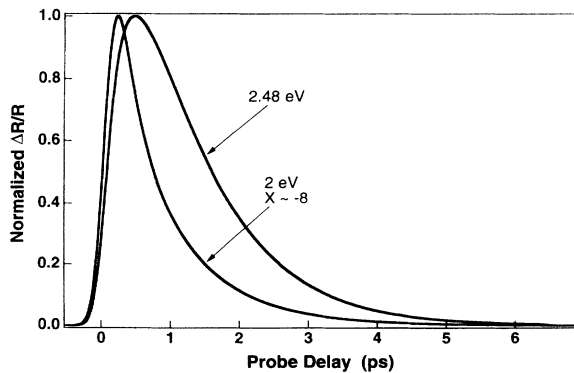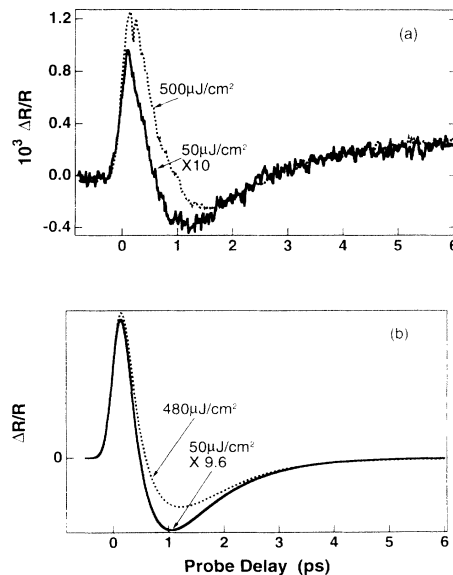

FIG. 13. Calculated transient differential reflectivity for a probe photon energy of 2 eV (solid line) and 2.48 eV (dashed line). The amplitudes have been normalized and maximum electronic temperature change ΔT_e^M is 40 K with pump fluence ~ 30 $\mu J/cm^2$.

FIG. 14. (a) Transient reflectivity measured for a probe photon energy of 2.68 eV with pump fluence 50 $\mu J/cm^2$ (solid line) and 500 $\mu J/cm^2$ (dashed line). (b) Transient reflectivity calculated for pump fluence of 50 $\mu J/cm^2$ (solid line) and 480 $\mu J/cm^2$ (dashed line) for the same probe photon energy.

connections between the probed parameters ($\Delta R/R$ and $\Delta T/T$) and the dielectric function changes [Eq. (2), Sec. II A]. The same time constants as in the 200-Å sample were found with $\tau_{\text{th}} = 500$ fs and $\tau_p = 1$ ps, indicating that the effect of diffusion can still be neglected on the time scale of our measurements. In the optically thick sample (1200 Å), ballistic transport of the electrons[12] takes place concurrently with electron-electron and electron-phonon mediated thermalization. The excited electrons move out of the skin depth region leading to a fast decay of the heating source (on typically less than 200 fs for a 1200-Å sample[12]) and to a large reduction of the amplitude of the reflectivity change.[19] In addition, longitudinal energy flow reduces the thermal contribution and results in a larger relative contribution from the short delay transient nonthermal electron distribution. The rise time of the transient reflectivity is consequently much faster and is limited by the temporal resolution of our experimental system.[19] The probe wavelength dependence of the transient reflectivity in this last sample is similar to that in the thin samples except for a further shift of the line shape toward higher probe energies.

V. CONCLUSION

The femtosecond transient reflectivity and transmissivity of optically thin gold films were investigated using a multiple-wavelength pump-probe technique. After perturbation of the electron distribution by free-carrier absorption of infrared femtosecond pulses, the electron-thermalization dynamics are followed by probing the optical properties at the second harmonic of the pump beam in the vicinity of the d band to the Fermi-surface transition. For short time delays (≤ 1 ps), the transient responses are deeply influenced by the nonthermal character of the broad electron distribution excited by the pump beam and cannot be interpreted with a model assuming instantaneous internal thermalization of the electron gas. In the vicinity of the spectral peak of the induced differential reflectivity and transmissivity, a slow rise of the signal is measured which is connected to the internal thermalization of the electron gas. Far off this peak the short time delay signal is very sensitive to the actual shape of the electron distribution leading to faster signal rise times and complex temporal responses which are direct signatures of the nonthermal character of the transient electron distribution. In the low perturbation regime investigated in our experiments, the results are directly connected to the temporal behavior of the electron distribution, permitting a precise access to the dynamics of electron distribution.

We have modeled the electron distribution dynamics using an extension of the classic two-temperature model assuming that the electron distribution changes can be separated into a Fermi (thermalized) and a non-Fermi (nonthermalized) component, coupled by energy exchanges through electron-electron interactions. In spite of the simplicity of this model, which considers only integrated energy exchanges, a good qualitative description of the observed dynamic behavior is obtained, permitting extraction of characteristic electron-thermalization times and yielding simple physical insight into the electron dynamics in metals. The measured data were reproduced over a large probe photon energy range using a characteristic electron-thermalization time of the order of 500 fs which has been found to be independent of the laser fluence in the range 2.5–200 μJ/cm^2 (i.e., estimated $\Delta T_e^M \sim 3$–200 K). Around the Fermi energy, a longer electron-thermalization time ~ 1–2 ps was observed, indicating inhibition of the electron-electron scattering close to the Fermi surface.

In order to get a more quantitative description of the measurements, a simulation based on numerical solutions of the Boltzmann equation has been developed to calculate the energy-dependent relaxation dynamics of the electron distribution. The calculated transient reflectivity and transmissivity show excellent agreements with the measured ones for a full thermalization time of the electron gas of the order of 1.5 ps. Away from the peak of optical changes, the contribution from the final thermal electron distribution is comparable to that from the short time nonthermal distribution. Thus for short delay time the behavior of $\Delta R/R$ and $\Delta T/T$ are dominated by the evolution of the initial electron distribution to a Fermi-Dirace distribution, resulting in a fast transient associated to redistribution of the perturbed electrons. In particular for probing with 2-eV photons, the transient differential reflectivity is calculated to rise almost instantaneously (for the time duration of the pulses used in our experiments), in agreements with previous measurements.[8,9,11,12] Studies using different sample thickness show good agreements with theoretical predictions, with the thermalization process in optically thick sample dominated by hot-electron transport.

The long electron-thermalization time we measured for a degenerated system is mostly due to state filling effects, which block the relaxation of electrons close to the Fermi surface while high-energy electrons decay on a much shorter time scale. Because the thermalization time is comparable to the phonon interaction time, internal and external thermalizations of the electron gas occur concurrently in nobel metals for which electron-phonon coupling is relatively weak. For metals with larger electron-lattice coupling, electron-phonon interactions should thus be treated in the nonequilibrium regime for electrons. The theoretical and experimental techniques developed in this study can form the basis for investigating and understanding nonthermal electronic effects in a wide range of metals.

ACKNOWLEDGMENTS

[1] S. I. Anisimov, B. L. Kapeliovich, and T. L. Perel'man, Zh. Eksp. Teor. Fiz. **66**, 776 (1974) [Sov. Phys. JETP **39**, 375 (1974)].

[2] G. L. Eesley, Phys. Rev. Lett. **51**, 2140 (1983).

[3] J. G. Fujimoto, J. M. Liu, E. P. Ippen, and N. Bloembergen, Phys. Rev. Lett. **53**, 1837 (1984).

[4] H. E. Elsayed-Ali, T. B. Norris, M. A. Pessot, and G. A. Mourou, Phys. Rev. Lett. **58**, 1212 (1987).

[5] R. W. Schoenlin, W. Z. Lin, J. G. Fujimoto, and G. L. Eesley, Phys. Rev. Lett. **58**, 1680 (1987).

[6] R. H. M. Groeneveld, R. Sprik, and A. Lagendijk, Phys. Rev. Lett. **64**, 784 (1990).

[7] S. D. Brorson, A. Kazeroonian, D. W. Face, T. K. Cheng, G.L. Doll, M. S. Dresselhaus, G. Dresselhaus, E. P. Ippen, T. Venkatesan, X. D. Wu, and A. Inam, Solid State Commun. **74**, 1305 (1990).

[8] H. E. Elsayed-Ali, T. Juhasz, G. O. Smith, and W. E. Bron, Phys. Rev. B **43**, 4488 (1991).

[9] T. Juhasz, H. E. Elsayed-Ali, X. H. Wu, and W. E. Bron, Phys. Rev. B **45**, 13 819 (1992).

[10] R. H. M. Groeneveld, R. Sprik, and A. Lagendijk, Phys. Rev. B **45**, 5079 (1992).

[11] S. D. Brorson, A. Kazeroonian, J. S. Moodera, D. W. Face, T. K. Cheng, E. P. Ippen, M. S. Dresselhaus, and G. Dresselhaus, Phys. Rev. Lett. **64**, 2172 (1990); S. D. Brorson, Ph.D. thesis, Massachussetts Institute of Technology, 1990.

[12] S. D. Brorson, J. G. Fujimoto, and E. P. Ippen, Phys. Rev. Lett. **59**, 1962 (1987).

[13] T. Juhasz, H. E. Elsayed-Ali, G. O. Smith, C. Suarez, and W. E. Bron, Phys. Rev. B **48**, 15 488 (1993).

[14] M. Mihailidi, Q. Xing, K. M. Yoo, and R. R. Alfano, Phys. Rev. B **49**, 3207 (1994).

[15] M. I. Kaganov, I. M. Lifshitz, and L. V. Tanatarov, Zh. Eksp. Teor. Fiz. **31**, 232 (1957) [Sov. Phys. JETP **4**, 173 (1957)].

[16] P. B. Allen, Phys. Rev. Lett. **59**, 1460 (1987).

[17] W. S. Fann, R. Storz, H. W. K. Tom, and J. Bokor, Phys. Rev. Lett. **68**, 2834 (1992).

[18] W. S. Fann, R. Storz, H. W. K. Tom, and J. Bokor, Phys. Rev. B **46**, 13 592 (1992).

[19] C.-K. Sun, F. Vallée, L. Acioli, E. P. Ippen, and J. G. Fujimoto, Phys. Rev. B **48**, 12 365 (1993).

[20] N. E. Christensen and B. O. Seraphin, Phys. Rev. B **4**, 3321 (1971).

[21] N. V. Smith, Phys. Rev. B **3**, 1862 (1971).

[22] P. B. Corkum, F. Brunel, and N. K. Sherman, Phys. Rev. Lett. **61**, 2886 (1990).

[23] R. Rosei, F. Antonangeli, and U. M. Grassano, Surf. Sci. **37**, 689 (1973).

[24] R. Rosei, Phys. Rev. B **10**, 474 (1974).

[25] F. Abelés, in *Advanced Optical Techniques,* edited by Van Heel (North-Holland, Amsterdam, 1967), Chap. 5, p. 144.

[26] P. B. Johnson and R. W. Christy, Phys. Rev. B **6**, 4370 (1972).

[27] D. W. Snoke, W. W. Rüle, Y. C. Lu, and E. Bauser, Phys. Rev. B **45**, 10 979 (1992).

[28] N. W. Ashcroft and N. D. Mermin, *Solid State Physics* (Holt-Saunders, Orlando, 1976).

[29] S. M. Sze, C. R. Crowell, G. P. Carey, and E. E. LaBate, J. Appl. Phys. **37**, 2690 (1966).

[30] L. H. Acioli, M. Ulman, F. Vallée, and J. G. Fujimoto, Appl. Phys. Lett. **63**, 666 (1993).

[31] D. S. Kim, J. Shah, J. E. Cunningham, T. C. Damen, S. Schmitt-Rink, and W. Schäfer, Phys. Rev. Lett. **68**, 2838 (1992).